

Identifying OH Imposters in the ALFALFA Neutral Hydrogen Survey

Katherine A. Suess,^{1,2*} Jeremy Darling,¹ Martha P. Haynes³ and Riccardo Giovanelli³

¹*Center for Astrophysics and Space Astronomy, Department of Astrophysical and Planetary Sciences, University of Colorado, 389 UCB, Boulder, CO 80309-0389, USA*

²*Department of Astronomy, University of California, Berkeley, 501 Campbell Hall, MC 3411, Berkeley, CA 94720-3411, USA*

³*Cornell Center for Astrophysics and Planetary Science, 616A Space Sciences Building, Cornell University, Ithaca, NY 14853, USA*

Accepted 2016 March 16. Received 2016 March 09; in original form 2016 February 11.

ABSTRACT

OH megamasers (OHMs) are rare, luminous molecular masers that are typically observed in (ultra) luminous infrared galaxies and serve as markers of major galaxy mergers. In blind emission line surveys such as the Arecibo Legacy Fast Arecibo L-Band Feed Array (ALFALFA) survey for neutral hydrogen (H I), OHMs at $z \sim 0.2$ can mimic $z \sim 0.05$ H I lines. We present the results of optical spectroscopy of ambiguous H I detections in the ALFALFA 40% data release detected by the Wide Field Infrared Survey Explorer (WISE) but with uncertain optical counterparts. The optical redshifts, obtained from observations at the Apache Point Observatory, revealed five new OHMs and identified 129 H I optical counterparts. Sixty candidates remain ambiguous. The new OHMs are the first detected in a blind spectral line survey.

The number of OHMs in ALFALFA is consistent with predictions from the OH luminosity function. Additionally, the mid-infrared magnitudes and colors of the OHM host galaxies found in a blind survey do not seem to differ from those found in previous targeted surveys. This validates the methods used in previous IR-selected OHM surveys and indicates there is no previously unknown OHM-producing population at $z \sim 0.2$. We also provide a method for future surveys to separate OH megamasers from 99% of H I line emitters without optical spectroscopy by using WISE infrared colors and magnitudes. Since the fraction of OHMs found in flux-limited H I surveys is expected to increase with the survey's redshift, this selection method can be applied to future flux-limited high-redshift hydrogen surveys.

Key words: line: identification – masers – galaxies: distances and redshifts – galaxies: starburst – galaxies: spiral – radio lines: galaxies

1 INTRODUCTION

The first hydroxyl megamaser (OHM) was discovered by Baan, Wood, & Haschick (1982) in Arp 220. The luminosity of the galaxy's OH emission line exceeded $10^3 L_\odot$ (orders of magnitude more luminous than known galactic OH masers), leading to the rise of the term ‘megamaser’ to describe masers with isotropic line luminosities in the range $10^{1-4} L_\odot$. Early OHM surveys such as Baan, Haschick, & Schmelz (1985) focused on galaxies with bright radio continuum and found <20 OHMs. After the launch of IRAS, surveys such as Staveland-Smith et al. (1992) and Norris, Gardner, & Whiteoak (1998) used IR properties to select ULIRG-like candidates with flat far-IR spectral indices and steep mid-IR spectral indices; these surveys discovered ~30 OHMs. Darling & Giovanelli (2000), Darling & Giovanelli (2001), and Darling & Giovanelli (2002a) (hereafter the Arecibo Megamaser Survey) carried out a deep survey using IR selection crite-

ria that roughly doubled the number of known OHMs. There are ~110 known OHMs up to $z = 0.264$, most of which are listed in Darling & Giovanelli (2002a).

All known OHMs are found in (ultra) luminous infrared galaxies ([U]LIRGs), extreme starburst galaxies that are almost exclusively the products of major galaxy mergers (Clements et al. 1996). Merger phase is correlated with the far infrared (FIR) luminosity of ULIRGs, and the OHM fraction in ULIRGs is a strong function of the FIR luminosity (Baan, Salzer & LeWinter 1998); this suggests that the presence of an OHM in a ULIRG indicates the phase of the merger. OHMs are also associated with high dense molecular gas fractions (Darling 2007), further indicating their relation to merger phase. Because OHMs are observable at large distances, they could provide a useful tracer of the galaxy merger rate as a function of redshift. Zeeman splitting of the OH line has also been observed in several OHMs (Robishaw, Quataert, & Heiles 2008), allowing for direct measurement of magnetic fields in star-forming regions.

While OHMs are interesting in their own right, they can also contaminate in blind emission line surveys for neutral hydrogen

* E-mail: suess@berkeley.edu

(H I). If $v_{\text{H I},0}/(1+z_{\text{H I}}) = v_{\text{OH},0}/(1+z_{\text{OH}})$, OH and H I lines appear at the same frequency and OHMs can be mis-identified as H I sources. While the fraction of OHMs in low-redshift H I surveys is small, this fraction is expected to increase with redshift and reach 50% by $z = 1$ (Briggs 1998). It is therefore necessary to develop a method to separate OH and H I lines in blind spectral line surveys before the advent of high-redshift H I surveys (e.g. ASKAP, Johnston et al. 2008).

In this work, we present the first OHMs detected in a blind spectral line survey. Five new OHMs at $0.167 \leq z_{\text{OH}} \leq 0.244$ were detected in the 40% data release of the Arecibo Legacy Fast Arecibo L-Band Feed Array Survey (ALFALFA, Haynes et al. 2011), a blind emission line survey for H I at $z \leq 0.06$. After confirming that the number and IR properties of these OHMs match empirical predictions, we develop a method to separate OH from H I lines without the use of optical spectroscopy.

Throughout this work, we assume a Λ CDM cosmology with $\Omega_m = 0.29$, $\Omega_\Lambda = 0.71$, and $H_0 = 70 \text{ km s}^{-1} \text{ Mpc}^{-1}$ (Hinshaw et al. 2013).

2 OBSERVATIONS AND DATA REDUCTION

We identified a total of 194 objects as potential OHMs by selecting objects from the ALFALFA 40% data release (Haynes et al. 2011) that had no optical counterpart velocity or an optical velocity that differed from the H I velocity by more than 300 km s^{-1} . We rejected large spiral galaxies that are clearly H I emitters. When more than one possible optical counterpart fell within the ALFALFA position ellipse, we selected the closest WISE mid-IR counterpart detected at $22 \mu\text{m}$ for optical spectroscopy.

We observed candidate OHMs at the Apache Point Observatory over 15 sessions between December 2011 and March 2013. Observations were made using the Dual Imaging Spectrograph at the Apache Point Observatory (APO) 3.5 m telescope with the B400/R300 grating and a 1.5" spectroscopic slit. This setup has a dichroic wavelength of $\sim 5350 \text{ \AA}$ and a resolving power of $R \sim 3250$ on the red side and $R \sim 2400$ on the blue side. Most targets had 2-4 observed frames, for a total exposure time of 5-20 minutes for typical objects and 1-2 hours for the faintest targets. Calibration images included bias frames, quartz lamp flat field frames, and spectra of helium, neon, and argon arc lamps for wavelength calibration.

Data reduction followed standard procedures for the IRAF ‘longslit’ package. Upper bounds for the pixel- \AA axis transformation uncertainty were 4 km s^{-1} on the red side and 21 km s^{-1} on the blue side. We adjusted the wavelength solution to heliocentric velocity using ‘rvcorrect’ and ‘dopcor’; this process added around 1 km s^{-1} of uncertainty in the wavelength solutions. Upper bounds for the wavelength calibration uncertainty were 125 km s^{-1} on the blue side and 92 km s^{-1} on the red side. After calibration, we aligned and median stacked exposures of the same science target.

We made line measurements using the IRAF ‘splot’ task. The red side of the spectrum usually showed H α (6563 \AA) bracketed by two [NII] lines (6549 and 6583 \AA), with a [SII] doublet (6717 and 6731 \AA) on the redward side. On the blue side, the most common lines were H β (4861 \AA) and two [OIII] lines (5007 and 4959 \AA). We also commonly observed other lines in the Balmer series of hydrogen as well as the 3727 \AA [OII] line on the blue side. Most objects had at least 5-7 observed optical lines, with 9 lines common. Only in a few cases were fewer than 5 lines observed. We measured RMS noise for each target in clean regions of the spectrum, away from astronomical sources, night sky lines, and cosmic

rays. We calculated final redshifts using an error-weighted average of the individual line measurements. The typical final uncertainty in redshift was 2×10^{-6} , or 0.6 km s^{-1} . The maximum centroid uncertainty observed was 5.4×10^{-5} , or 16 km s^{-1} .

Typical and maximum values for all factors contributing to the final uncertainty in measured velocities are: instrumental uncertainty, 112 km s^{-1} typical and 125 km s^{-1} maximum; wavelength calibration, 13 km s^{-1} typical and 21 km s^{-1} maximum; heliocentric calibration, 1 km s^{-1} maximum; and line centroid uncertainty, 1 km s^{-1} typical and 16 km s^{-1} maximum. Adding these uncertainties in quadrature, we arrive at 113 km s^{-1} typical uncertainty and 128 km s^{-1} maximum uncertainty. We thus conservatively adopt 130 km s^{-1} as the uncertainty on all optical recession velocity measurements.

3 RESULTS

For each observation, we could make one of three determinations. The first, and most common, was that the velocity of the observed object matched (within uncertainty) the velocity listed in the ALFALFA catalog. It was also possible for the object’s velocity to match the OH velocity, found by recalculating the velocity in the ALFALFA catalog using an OH rest frequency instead of an H I rest frequency:

$$z_{\text{OH}} = \frac{v_{\text{OH},0}}{v_{\text{H I},0}}(1 + z_{\text{H I}}) - 1, \quad (1)$$

where $z_i = v_i/c$ and we adopt a frequency of 1667.35903 MHz for OH and 1420.405752 MHz for H I. These objects are OHMs. The third possible outcome was ambiguous, where the observed velocity matched neither the H I nor the OH velocity. These ambiguous cases are observations of the incorrect optical counterpart or of a false positive ALFALFA detection.

3.1 OH Detections

We identified five previously undiscovered OHMs through APO observations. Additionally, Haynes et al. (2011) identified one previously discovered OHM (AGC 181310, IRAS 08201+2801, discovered by Darling & Giovanelli 2001) in the ALFALFA $\alpha.40$ release. These six objects are the only known OHMs in the ALFALFA $\alpha.40$ database. Extrapolating to the full sample size indicates ALFALFA will detect on the order of 15 total new OHMs, slightly lower than Giovanelli et al. (2005) predictions that the survey ‘should detect several additional dozen OHMs.’ Table 1 lists the optical, OH, and H I velocities for the six ALFALFA OHMs as well as the line peak and width from ALFALFA (Haynes et al. 2011). ALFALFA extracts line peaks and widths using a matched-filtering approach described in Saintonge (2007); the templates used are Hermite functions. Table 2 lists the infrared properties of the OHMs. Figure 1 shows the spectra of the six OHMs.

3.2 H I confirmations

We confirmed 129 H I sources with APO observations. For each, we noted the exact location of the optical counterpart—these occasionally differed slightly from the ALFALFA location due to the survey’s large beam. We used SDSS DR9 in conjunction with telescope pointing images taken during APO observations to confirm the J2000 coordinates of the H I optical counterpart, and APO telescope pointing images to confirm the positions of the few objects

Table 1. OH Megamasers detected in the ALFALFA 40% survey. Optical velocities were obtained from APO observations; all uncertainties are 130 km s^{-1} . H I velocities are taken from the ALFALFA $\alpha.40$ data release (Haynes et al. 2011), with uncertainties in parentheses. OH velocities are calculated from the H I velocities using Equation 1, with uncertainties in parentheses. The bolded OHM was discovered in the $\alpha.40$ data release by Haynes et al. (2011).

Object Name	Position (J2000)	Optical Velocity (km s^{-1})	H I Velocity (km s^{-1})	OH Velocity (km s^{-1})	Line Peak (mJy)	Line Width (km s^{-1})
015001+240236	015001.57+240235.8	61268	7775(32)	61249(38)	9(2)	468(64)
022657+282457	022657.65+282457.5	64397	10185(11)	64078(13)	11(3)	158(22)
AGC 181310	082312.7+275138	50365	-1551(13)	50302(15)	19(2)	193(26)
AGC 219215	111125.06+052046.0	67517	13148(2)	67556(2)	21(2)	45(4)
145537+062437	145537.39+062437.4	68960	13749(5)	68262(6)	8(2)	83(9)
AGC 257959	155537.94+143905.6	61028	7393(2)	60801(2)	20(2)	206(5)

Table 2. Luminosity and IR properties of OH Megamasers detected in the ALFALFA 40% survey. OH luminosity is calculated from the ALFALFA detection, and the far infrared (FIR) luminosity is derived from the 60 and $100 \mu\text{m}$ IRAS fluxes according to the prescription in Fullmer & Lonsdale (1980). The notation [22] refers to the Vega magnitude measured at $22 \mu\text{m}$.

Object Name	$\log(\frac{L_{\text{OH}}}{L_{\odot}})$	WISE [3.4]	WISE [4.6]	WISE [12]	WISE [22]	IRAS $f_{60\mu\text{m}}$ (Jy)	IRAS $f_{100\mu\text{m}}$ (Jy)	$\log(\frac{L_{\text{FIR}}}{L_{\odot}})$
015001+240236	3.61	14.23	13.61	9.82	7.47	0.301	1.064	11.87
022657+282457	3.29	13.39	12.55	9.43	7.29	—	—	—
AGC 181310	3.33	14.20	13.22	8.33	5.02	1.171	1.430	11.97
AGC 219215	3.26	15.15	13.99	9.94	7.59	—	—	—
145537+062437	3.06	14.60	13.72	9.54	6.60	0.470	1.388	12.14
AGC 257959	3.60	14.91	13.54	9.39	7.09	0.743	1.194	12.10

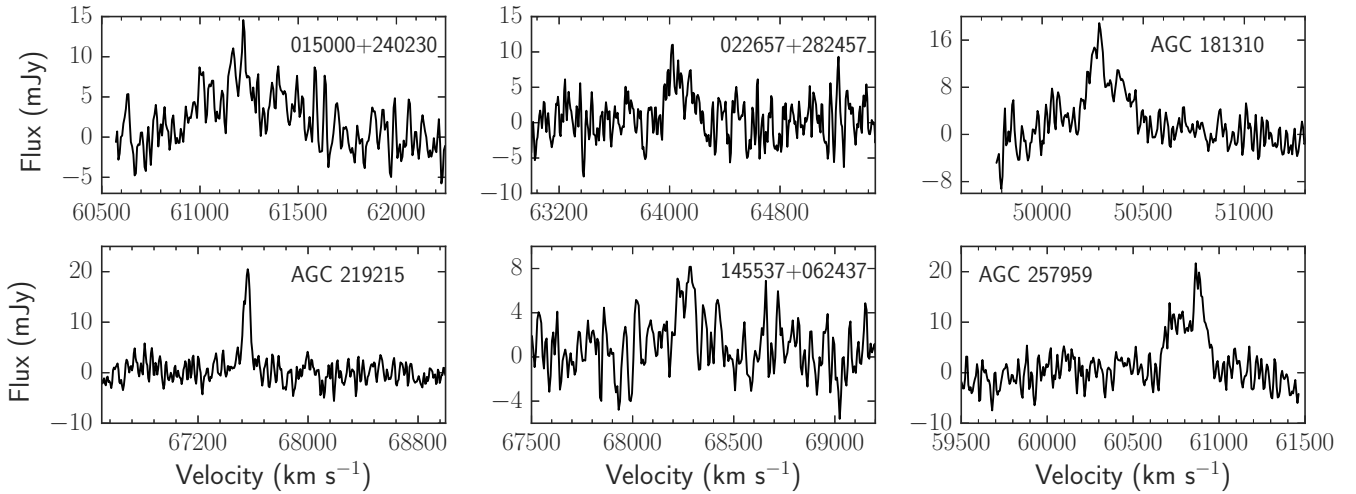


Figure 1. ALFALFA spectra of the six OH megamasers confirmed with APO observations. The velocity axis indicates the heliocentric optical velocity of the OH 1667 MHz line.

that did not fall within the Sloan sky coverage. In Table 3, we list all identified H I sources with their name (6-numeral strings represent AGC name), optical position, optical velocity, and ALFALFA velocity.

3.3 Ambiguous Optical Counterparts

Sixty objects remained ambiguous after APO observations: velocities for these objects matched neither H I nor OH velocities, or no optical lines were detected. Many of the observed OHM candidates were not high signal-to-noise ALFALFA detections, and the majority of the ambiguous optical counterparts are likely false positive ALFALFA detections. When multiple possible optical counterparts

appeared within the ALFALFA beam radius, we made observations of the object brightest in the WISE 22 μm band; some of the ambiguous optical counterparts likely correspond to observations of a different object than the ALFALFA emitter. Several ambiguous objects had no observable optical lines. Table 4 lists ambiguous optical counterparts.

4 ANALYSIS & DISCUSSION

4.1 ALFALFA OH Completeness

For the survey to be ‘complete’ with respect to OHMs, ALFALFA should have detected all previously known OHMs within the sur-

Table 3. Optical counterpart redshifts of H I-emitting galaxies. Six-digit object names are AGC names. H I velocities are from Haynes et al. (2011), with uncertainties in parentheses.

Object Name	Optical Counterpart Position (J2000)	Optical Velocity ¹ (km s ⁻¹)	H I Velocity (km s ⁻¹)
102733	000129.98+311402.9	12660	12581(6)
100783	000347.49+312037.7	5065	5011(4)
102902	000948.86+284123.8	10688	10560(4)
107	001138.10+275652.8	7488	7437(3)
102643	002136.21+252931.1	6960	7042(13)
102644	002251.57+254720.2	7188	7018(10)
HI003023+251839	003023.94+251903.8	7424	7295(7)
100291	003212.12+312459.5	6232	6140(30)
102301	004342.83+255150.1	5167	5180(5)
102935	004825.32+284535.4	4475	4400(10)
101685	010034.02+270552.7	11216	11040(4)
113892	010105.79+310419.4	6677	6714(3)
748808	010908.52+141358.4	9551	9551(3)
113924	012626.02+310032.5	13646	13470(3)
114047	013326.39+285623.4	7801	7700(8)
113941	014140.52+312946.6	10975	10741(2)
114121	014636.92+144131.0	7462	7485(2)
748822	015224.00+154101.6	13036	12866(8)
113956	015327.57+305349.9	11353	11205(2)
113964	015521.61+313730.4	4634	4486(3)
123118	020149.86+292647.7	16988	16909(16)
122960	020426.95+310734.6	4907	4787(4)
HI020624.2+160545	020626.40+160538.1	5308	5346(4)
748838	020948.79+153345.1	10934	10774(4)
748840	021022.44+144415.7	17764	17578(11)
122141	021133.13+141419.4	3807	3797(3)
123103	021145.35+311130.2	4740	4819(5)
121499	021228.93+291057.9	9996	9920(5)
122979	021513.92+310533.3	5007	4968(11)
122855	021847.24+145042.8	3996	3907(2)
122988	021954.56+295050.3	11230	11080(12)
122194	022139.74+280307.2	10783	10642(4)
120193	022255.51+251827.4	4665	4584(10)
123143	022312.08+282722.9	10321	10295(3)
122859	022451.18+161039.3	8291	8189(3)
123005 ²	022542.30+313722.9	5035	5159(20)
120240	022555.82+245125.0	10890	10799(8)
121216	022558.74+271613.5	10345	10171(42)
123158	023006.35+284027.2	11120	10958(2)
122883	023141.96+241720.6	5338	5409(8)
122214	023233.70+275626.8	4777	4657(7)
123163	023245.42+283318.5	10678	10660(7)
122215	023328.44+271140.9	5471	5343(7)
120342	023346.91+301121.5	10339	10253(5)
2155	024005.68+142233.3	13893	13911(3)
122421	024131.69+263742.9	1566	1586(3)
748875	024604.91+143916.1	7580	7541(13)
122850	024639.50+150856.6	7828	7791(3)
122857	024703.76+145052.0	7761	7598(2)
120529	024853.52+281624.8	5432	5424(6)
748888	024922.00+150223.7	8824	8819(32)
749015	025303.78+143739.3	9829	9891(33)
122809	025905.53+271055.4	10853	10842(10)
122810	025929.19+255351.4	10358	10402(5)
123065	025959.37+305912.8	5924	5971(2)
748916	030647.43+143633.0	10105	10014(4)

¹The uncertainty on optical velocities is 130 km s⁻¹ for all objects.²This spectrum showed both emission and absorption lines. The emission lines were more prevalent, but the offset absorption lines clearly showed in the blue half of the spectrum. Absorption was especially evident in H β and blueward Balmer series lines, where broad emission lines were nearly divided in two by the offset absorption. The emission velocity occurred at 5035 km s⁻¹, a match for the ALFALFA H I line; the absorption lines were offset to 5770 km s⁻¹. The velocity listed in Table 3 is the emission velocity, which matches the ALFALFA H I velocity. The galaxy exhibits disturbed morphology in SDSS, and the absorption and emission lines may be offset because they come from different nuclei.

Table 3 – *continued* Optical Counterpart Redshifts of H I-Emitting Galaxies.

Object Name	Optical Counterpart Position (J2000)	Optical Velocity (km s ⁻¹)	H I Velocity (km s ⁻¹)
748918	030715.30+151745.7	5687	5659(8)
174684	073019.16+060634.9	8502	8504(2)
174697	073532.66+062646.3	9719	9755(3)
174481	073602.49+133216.4	4740	4770(4)
174491	073732.29+125218.4	13970	13973(5)
170347	074035.08+260806.1	8394	8383(7)
182739	080247.11+244617.0	12463	12379(25)
188943	080520.82+055706.6	9055	9100(34)
180967	081425.34+042032.9	10117	10275(6)
749273	081709.90+263354.2	5817	5838(4)
182496	082626.06+044839.2	8531	8525(2)
183495	082907.22+275655.0	12525	12568(11)
184464	085402.71+275730.5	8094	8006(6)
749210	113201.37+272451.2	15203	15050(3)
215140	114201.25+134155.5	4435	4259(4)
HI122922+042247 ³	122922.81+042246.1	4999	5009(4)
221030	124835.53+090732.3	7711	7558(4)
238878	130212.70+110034.0	13636	13689(36)
230239	131928.51+143439.4	6787	6705(6)
238831 ⁴	132102.19+260833.4	17192	17081(4)
749554	132537.83+244712.5	10094	10076(4)
233819	135106.13+082038.9	6971	6915(13)
241309	140437.88+152832.0	7904	7786(9)
240736	144934.54+111453.1	16212	16426(4)
249263 ⁵	145233.39+060115.3	East: 14196	14327(3)
	145235.88+060128.6	South: 14452	
248894	145949.34+152421.3	13621	13528(7)
258105	150157.30+091118.1	8988	8895(17)
258530	150834.82+265155.4	17523	17513(29)
257884	151333.16+121211.0	16638	16696(4)
727058	151956.28+253618.2	9789	9695(30)
257934	154349.18+143856.7	10440	10363(9)
258337	154555.99+043249.7	6499	6440(1)
257961	155637.52+160224.1	4617	4538(4)
268208	162934.08+040227.3	16315	16255(4)
268223	162942.53+055505.3	9912	9866(3)
748649	214534.16+135511.8	8774	8788(39)
310185	215016.37+155234.8	7597	7520(3)
310204	215252.88+153418.5	13363	13169(3)
748661	215352.36+160637.2	7840	7691(3)
321219	220954.17+263157.1	11443	11355(7)
321410	221133.62+305412.1	4934	4805(4)
321209	222121.00+275033.3	12665	12706(13)
320185	222355.67+151447.3	7398	7318(3)
321344	223531.15+251040.0	12220	12108(3)
321284	223827.40+255502.7	8761	8593(11)
748716	224105.61+154923.9	1935	1936(3)
321487	224230.83+293229.8	7475	7314(5)
320379	224833.94+243205.0	12441	12319(12)
321440 ⁶	225030.19+315112.5	6418	6462(1)
321453	225720.88+315316.0	6682	6660(5)
332908	230543.41+271245.7	7457	7406(3)
332417	230636.70+141014.7	12150	11962(6)
333370	231422.07+311503.4	7286	7235(9)
HI231551+253430	231551.33+253428.5	9900	9829(16)
333634	231643.23+244148.4	17193	17155(141)
333525	232017.84+290859.5	6117	5956(17)

³This object was identified as a clear H I detection; in SDSS it appears to be a blue compact dwarf galaxy.⁴The optical counterpart for this object was confirmed to be the blue extended object to the west of the central ALFALFA coordinates.⁵Two objects were observed within the ALFALFA beam radius. One observed galaxy was to the east of the ALFALFA target coordinates, and one to the south. Both galaxies matched the H I velocity, so the coordinates and measured velocities for both are included in this table.⁶Most observed objects have at least five identifying spectral lines. For this object, only H α was identified. Despite the scarcity of observable optical lines in this spectra, we are confident of the H I confirmation. The singular line is bright, shows extension along the spatial axis of the spectrum, and it is very close to the expected H I redshift. In visible light, the object appears to be a low surface brightness galaxy.

Table 3 – *continued* Optical Counterpart Redshifts of H I-Emitting Galaxies.

Object Name	Optical Counterpart Position (J2000)	Optical Velocity (km s ⁻¹)	H I Velocity (km s ⁻¹)
333331	232510.17+245047.8	9766	9748(4)
333286	232551.71+253820.8	8732	8582(21)
333538	232637.07+294125.1	6837	6788(3)
333392	232708.90+302417.9	4541	4521(4)
333460	232854.66+310459.5	13637	13641(7)
333398	232947.28+301524.8	8393	8269(8)
331198	233211.07+285731.5	5615	5512(23)
12658	233244.79+310649.4	9615	9502(2)
331305	234324.28+265457.3	8252	8189(5)
333419	234411.82+314557.8	9395	9319(5)
333566	234557.53+290958.4	9784	9694(40)
333232	234628.30+274423.6	8106	8092(2)
333205	234629.34+274131.6	16815	16873(12)
331380	235347.85+253529.7	11423	11510(10)
333220	235529.44+275902.3	9191	9015(6)
333436	235648.68+302422.5	9455	9331(11)
333239	235916.84+274521.4	14615	14586(5)

vey flux, area, and redshift limits; furthermore, the number of OHM detections should match predictions from the OH luminosity function (OHLF, [Darling & Giovanelli 2002b](#)). Analysis of ALFALFA OH completeness provides a test of the OHLF in a blind survey, assesses the sensitivity of a blind H I survey like ALFALFA to OHMs, and may provide guidance for future H I surveys.

[Darling & Giovanelli \(2000\)](#) lists the majority of the ~ 120 OH megamasers known prior to this work; only 8 of these previously known masers lie within the volume defined by the ALFALFA 40% sky coverage (listed in [Haynes et al. 2011](#)) and depth ($0.167 \leq z_{OH} \leq 0.244$). Maser spectra from the Arecibo Megamaser Survey show that only one of the eight previously known masers in the ALFALFA volume is above the survey’s S/N detection limit of 4.6. This OHM, AGC 181310/IRAS 08201+2801, was discovered by [Darling & Giovanelli \(2001\)](#) at $z = 0.1680$; it was indeed detected by ALFALFA (Table 1). The five new OHM detections presented in this work were not found in previous surveys because the objects did not yet have optical redshifts, which previous OHM surveys relied on for spectrometer tuning. While ALFALFA found all previously discovered OHMs within the constraints of the survey, it found only 12.5% of the known OHMs within its sky footprint. This indicates that future H I surveys must have lower detection thresholds than ALFALFA if detecting new OHMs is a secondary goal.

The OHLF ([Darling & Giovanelli 2002b](#)) describes the expected power-law luminosity density distribution of OHMs:

$$\phi = (9.8^{+31.9}_{-7.5} \times 10^{-6}) L_{OH}^{-0.64 \pm 0.21} \text{Mpc}^{-3} \text{dex}^{-1}. \quad (2)$$

We note that the OHLF was developed from the results of a targeted survey, the Arecibo Megamaser Survey. The ALFALFA results provide the first opportunity to test the OHLF against the results of a blind survey.

To integrate the OHLF and find the number of expected OHMs, we must compute the volume of the 40% ALFALFA data release as well as the survey’s luminosity limits. Using the Cosmology Calculator ([Wright 2006](#)), the comoving volume within ALFALFA’s redshift range is 3.17 Gpc^3 . The survey covers $\sim 6.8\%$ of the sky, so we use 0.21 Gpc^3 as the total volume of ALFALFA. The survey does not have a hard upper luminosity cutoff; however, the OHLF was calculated using data below $10^{3.8} L_{\odot}$. For this analysis, we choose an upper luminosity limit of $10^4 L_{\odot}$. This is close

enough to the bounds of the Arecibo Megamaser Survey that the OHLF should still be valid; furthermore, increasing the luminosity limit further will not dramatically change the number of additional OHMs expected due to the power-law luminosity drop off. ALFALFA’s S/N detection limit of 4.6 corresponds to a 7.7 mJy peak in narrow Gaussian lines like OH; this determines the survey’s lower luminosity limit. Assuming a Gaussian OH line with a line width of 150 km s^{-1} (typical for OHMs) and peak of 7.7 mJy, the integrated flux of the line is $0.87 \text{ Jy km s}^{-1}$. Assuming a distance corresponding to the maximum $z_{OH} \approx 0.25$ for ALFALFA, the lower luminosity bound is $10^{3.2} L_{\odot}$. However, this is not a hard lower cutoff; narrow lines could be detected below our luminosity cutoff and broad lines could remain undetected above our luminosity cutoff. It is not surprising, then, that ALFALFA OHM 145537+062437 has a luminosity of 3.06 dex, below the 3.2 dex cutoff. There are also reliability limitations at the low-flux limit— despite identifying candidate OHMs near $10^{3.2} L_{\odot}$, we could not measure optical redshifts for many of the faint optical counterparts and the objects remain in the ‘ambiguous’ category (Table 4).

Integrating Equation 2 from $10^{3.2} L_{\odot}$ to $10^{4.0} L_{\odot}$ over a volume of 0.21 Gpc^3 yields a prediction of 9^{+73}_{-8} OHMs in the ALFALFA $\alpha 40$ survey. We detected six OHMs in ALFALFA, well within the large error bars of our expectation. This indicates that OHMs found in a blind survey are consistent with the OHLF from the Arecibo Megamaser Survey. A plot of the OHLF and the distribution of observed OHMs is shown in Figure 2.

ALFALFA found all previously known OHMs within the survey detection limits and the total number of OHMs in the survey is consistent with empirical predictions from the OHLF. We can therefore say that, within error, the ALFALFA survey is complete with respect to OHMs.

4.2 Comparison of New and Existing OHMs

Previously detected OHMs were primarily found through targeted surveys (e.g. [Baan, Haschick, & Schmelz 1985](#); [Stavely-Smith et al. 1992](#); [Norris, Gardner, & Whiteoak 1998](#), Arecibo Megamaser Survey) that used IR selection criteria; however, this work makes use of a blind H I survey to find OHM candidates and does not rely on assumed IR characteristics. Comparing ALFALFA OHMs with previously discovered masers

Table 4. Ambiguous optical counterparts. Six-digit object names are AGC names. H I velocities are from Haynes et al. (2011), with uncertainties in parentheses. The designation ‘neither’ indicates that the observed velocity matches neither H I nor OH, while ‘no lines’ designates objects for which no optical lines were observable and no velocity determination could be made. ‘ML’ indicates that the ALFALFA H I detection is a marginal line, likely not a real detections. ‘UL’ indicates that the ALFALFA line is uncertain, and could be H I or another line.

Object Name	Observed Position (J2000)	Optical Velocity ¹ (km s ⁻¹)	H I Velocity (km s ⁻¹)	OH Velocity (km s ⁻¹)	Designation
HI000335.7+253214	000336.02+253204.0	-	-1319(7)	50573(8)	No Lines
102624	000903.33+252750.4	31506	1393(5)	53757(6)	Neither, UL
HI002048+294651 ²	002049.69+294651.5	-	6799(4)	60103(5)	Wrong Pointing
HI002957+305739 ³	002957.16+305744.3	22618	-596(5)	51423(6)	Neither
102983	003338.74+284526.0	-	3607(9)	56356(11)	No Lines
HI005058+284800	A:005058.30+284800.0; B:005059.40+284803.6	A: 87656; B: 87233	1255(20)	53595(23)	Neither, UL
102942	005355.45+290715.8	10936	11585(5)	65721(6)	Neither
HI005555+294810	005555.11+294836.2	107964	1038(9)	53341(11)	Neither, UL
102820 ⁴	005626.11+305408.2	5320	4776(21)	57729(25)	Neither
HI011145+290458	011142.86+290510.9	A: 28224; B: 28710	16654(18)	71672(21)	Neither, ML
HI011200+274341	011200.29+274342.0	33390	14232(3)	219192(4)	Neither, ML
HI012215+284810	012217.19+284753.0	4321	2161(4)	54659(5)	Neither
114080	013310.10+284520.3	193966	1865(29)	54311(34)	Neither, ML, AGN
113863	014339.23+260036.2	39842	3932(20)	56738(23)	Neither, ML
HI015722.6+144843 ⁵	015725.33+144813.9	-	7589(4)	61030(5)	Neither
113868	015838.90+250726.6	30843	1922(5)	54378(6)	Neither, ML
HI020827.4+154646	020828.15+154639.3	-	4701(4)	57640(5)	No Lines
HI021034.5+253405	021033.59+253327.5	-	17647(5)	72837(6)	No Lines
121286	021646.75+291236.2	18988	13052(10)	67443(12)	Neither, UL
HI022701.3+245402	022702.92+245421.2	64392	14966(20)	69690(23)	Neither, UL
122433	023126.73+255653.9	15836	14223(14)	68818(16)	Neither
HI073435.3+083500	073436.24+083500.6	47004	168(5)	52319(6)	Neither, UL
174555	074945.10+134554.5	29544	2416(7)	54958(8)	Neither, UL
HI080838.6+053210	080840.87+053140.4	-	9187(14)	62906(16)	No Lines
189051	085016.90+271219.0	29971	4515(4)	57422(5)	Neither, UL
219219	110416.13+045719.9	66771	7113(6)	60472(7)	Neither
219220	111301.97+040305.7	45550	6683(8)	59967(9)	Neither
215280	111316.20+152431.8	-	1479(2)	53858(2)	No Lines
215238	111519.91+114053.6	50092	3053(4)	55706(5)	Neither, UL
219222	111553.88+042227.9	24701	6218(28)	81118(33)	Neither, ML
HI113900.7+102250	113858.83+102222.5	73121	5118(5)	58130(6)	Neither, ML
HI115119.4+274818	115121.03+274827.0	26848	14191(5)	68780(6)	Neither, UL
HI124540+070337	124543.33+070329.2	-	-624(4)	51390(5)	No Lines
HI130227+135524	130226.79+135548.7	83292	13344(1)	67786(1)	Neither
HI134330.3+111234 ⁶	134332.00+111220.1	181209	1150(5)	53472(6)	Neither
248933	142413.05+143904.0	-	2459(3)	55008(4)	No Lines
249181	143426.77+093913.8	-	16288(11)	71242(13)	No Lines, UL
249244	144022.48+082122.3	-	8966(4)	62647(5)	No Lines
145944+102905	145944.89+102906.2	-	5884(3)	59029(4)	No Lines
150338+121443 ⁷	150342.94+121449.5	110830	2669(3)	55255(4)	Neither, UL
HI150423.7+240930 ⁸	150422.90+241004.6	-	1217(5)	53550(6)	Pointing Error
HI150900	150900.54+085536.6	22768	16663(31)	71682(36)	Neither, ML
258004	151236.29+151010.9	-	10552(4)	64508(5)	No Lines, ML
257889	151546.67+155336.6	50026	11193(4)	65261(5)	Neither
HI151620+152939	151620.26+152938.9	61857	12910(5)	67277(6)	Neither, UL
151659+051751	151659.24+051751.5	15363	2221(13)	54736(15)	Neither, ML
152933+150728	152933.22+150728.7	39468	5365(5)	58420(6)	Neither, UL
727130	152948.19+260516.3	-	2019(3)	54492(4)	No Lines
HI153050.1+123632	153052.73+123611.5	71904	629(4)	52861(5)	Neither, UL
HI153948.8+275213	153950.39+275247.9	-	9322(5)	63065(6)	No Lines, UL

¹The uncertainty on optical velocities is 130 km s⁻¹ for all objects.

²Possible pointing error during observations; this object may not be the WISE bright source or the ALFALFA detection.

³The α .40 data release of the ALFALFA catalog incorrectly states that this object is an OHM (Haynes et al. 2011). While the measured optical velocity is much higher than the ALFALFA velocity, it does not match the OH velocity and the object’s identity remains unknown.

⁴The velocity determination for this object was measured from only one line, presumed to be H α .

⁵Bleed-in from a nearby star obscured optical lines for this object.

⁶Two objects were observed within beam uncertainty of the ALFALFA detection. The first had no visible optical lines, and the second (the velocity listed in Table 4) showed broad line emission that matched neither the OH nor the H I velocity.

⁷Due to high redshift, this object is likely an AGN.

⁸Guiding errors during observing rendered these frames unusable; no further observations were made.

Table 4 – *continued* Ambiguous optical counterparts.

Object Name	Observed Position (J2000)	Optical Velocity ¹ (km s ⁻¹)	H I Velocity (km s ⁻¹)	OH Velocity (km s ⁻¹)	Designation
258212	154609.82+083131.0	40857	12576(6)	66885(7)	Neither, ML
HI154718.3+043350	154718.37+043346.7	-	5776(5)	58902(6)	No Lines, UL
268216	161222.06+063217.5	82218	1723(3)	54145(4)	Neither
268065	161643.74+151302.0	55184	10078(4)	63952(5)	Neither
HI215549.4+303121	215551.26+303056.1	-	24(1)	52151(1)	No Lines, UL
330051	230619.72+275337.8	-	6901(3)	60223(4)	No Lines
HI231619+253530	231616.19+253534.5	-	-1133(8)	50792(9)	No Lines
333281	232230.19+243525.0	-	9708(2)	63518(2)	No Lines; Star?
333335 ⁴	233419.25+250753.1	40996	5112(11)	58123(13)	Neither, UL
333476 ⁹	235925.00+302828.4	50343	12076(5)	66298(6)	Neither

⁴The velocity determination for this object was measured from only one line, presumed to be H α .

⁹Two possible optical counterparts were observed. One matched neither OH nor H I velocities, and the other had no clear optical lines.

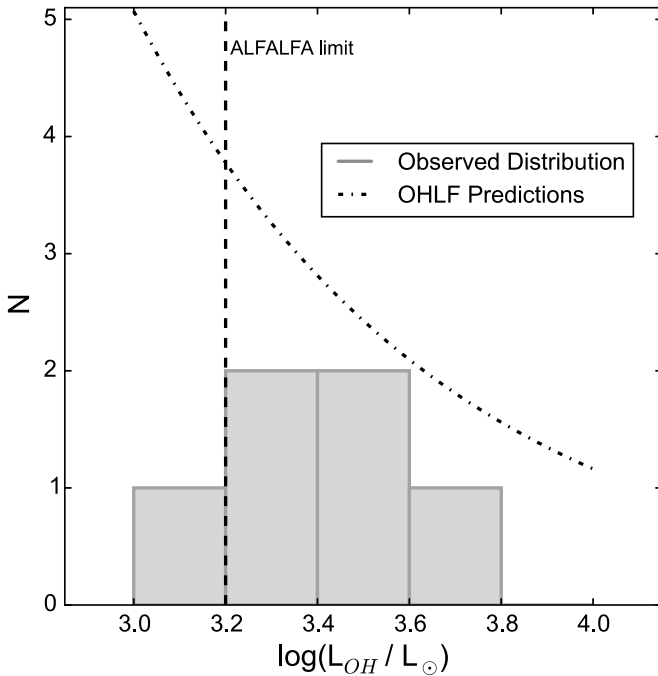


Figure 2. Number of OHMs as a function of luminosity. The histogram shows the observed ALFALFA OHM distribution; predictions from the OHLF are shown by the dashed line. Error bars on the OHLF curve are larger than the scale of the plot, and are not plotted.

thus provides an opportunity to verify the selection criteria used in previous targeted surveys and to test for a new OHM-producing environment at $z \sim 0.2$.

We use a two-sided Kolmogorov-Smirnov (K-S) statistical test to determine if the two OHM populations come from the same distribution in IR space. The OHM comparison sample consists of 109 OHM host galaxies identified in Baan, Salzer & LeWinter (1998) and the Arecibo Megamaser Survey. We use magnitudes and colors from the WISE All-Sky Source Catalog (Wright et al. 2010) as well as 60 and 100 μ m flux from IRAS (Saunders et al. 2000) and the FIR luminosity calculated from IRAS according to the prescription in Fullmer & Lonsdale (1980). IRAS did not detect ALFALFA OHMs AGC 219215 and 022657+282457, so they are not included in the K-S tests for IRAS 60 and 100 μ m flux or FIR luminosity; all previously known OHMs are detected in IRAS. K-S test p-values

Table 5. K-S tests for ALFALFA OHMs and previously discovered OHMs.

Infrared Property	K-S p-value
WISE [3.4]	0.123
WISE [4.6]	0.326
WISE [12]	0.175
WISE [22]	0.103
WISE [12] – [22]	0.038
WISE [4.6] – [12]	0.797
WISE [3.4] – [4.6]	0.174
IRAS 60 μ m flux	0.055
IRAS 100 μ m flux	0.015
$\log(L_{\text{FIR}}/L_{\odot})$	0.055

are shown in Table 5; all p-values are above 0.01, implying that the two populations do not show significant evidence for being drawn from different distributions. This indicates that the IR selection criteria used in previous targeted OHM surveys did not exclude a significant portion of the OHM population found in a blind survey; additionally, this work has not discovered a new population of OHMs missed by targeted surveys.

4.3 Distinguishing OH from H I

It is impossible to distinguish OH lines from H I lines using only H I survey spectra. OHMs at $z \sim 0.2$ have the same observed frequency as H I at $z \sim 0.05$, and the two radio lines are nearly indistinguishable. Example OH and H I lines from ALFALFA are shown in Figure 3.

Given that it is difficult to distinguish between H I and OH, how important is it for an H I survey to separate the two populations? Only $\sim 0.05\%$ of ALFALFA $\alpha 40$ objects are OHMs. However, this is mostly due to the survey’s low redshift range: the percentage of OH lines detected in an H I survey is expected to increase with redshift because thermal H I emission is mass-limited while OH maser amplification is not. Half of the detections from an H I survey at a redshift of $z = 1$ are expected to be OH lines (Briggs 1998).

Several high-redshift H I surveys (including ASKAP-WALLABY (Johnston et al. 2008), MeerKAT-LADUMA (Holwerda et al. 2011), and ultimately the Square Kilometer Array) are currently planned and in development. WALLABY will survey $z < 0.26$, while LADUMA and SKA aim to cover redshifts up to $z \sim 1$; all of these planned H I surveys will observe a much

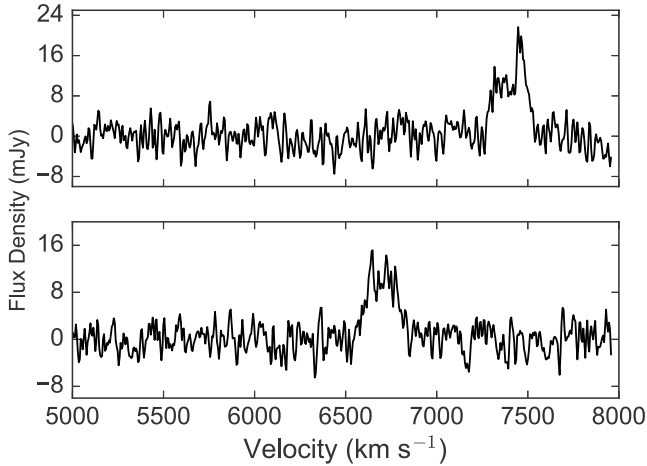


Figure 3. Two sample ALFALFA spectra showing flux density as a function of H I velocity (Haynes et al. 2011). Top is AGC 257959, an OH megamaser; bottom is AGC 230239, an H I emission line galaxy.

Table 6. K-S tests for ALFALFA OHMs and ALFALFA H I lines. Significant results are indicated in bold type, showing inconsistent [4.6]–[12] and [3.4]–[4.6] μm colors between the two populations.

Infrared Property	K-S p-value
WISE [3.4]	0.072
WISE [4.6]	0.379
WISE [12]	0.018
WISE [22]	0.552
WISE [3.4] – [4.6]	7.05×10^{-6}
WISE [4.6] – [12]	0.010
WISE [12] – [22]	0.024

larger population of OHMs than ALFALFA. Not only will locating OH lines in these surveys provide a larger and more robust sample of OHMs to further science goals such as tracking the galaxy merger rate as a function of redshift, it will also improve the fidelity of the survey catalogs. While OH lines in ALFALFA are not numerous, they are an excellent training set for distinguishing OH lines from H I lines without the use of optical spectroscopy.

We expect OHMs, almost exclusively found in dusty IR-bright galaxies, to show different IR properties than H I emitters. We used a K-S test in WISE colors and magnitudes to compare the 6 ALFALFA OHMs with ALFALFA H I sources detected by WISE. We matched ALFALFA sources to the WISE All-Sky Source Catalog within a 45 arcsecond radius, requiring signal-to-noise > 5 at 3.4, 4.6, and 12 μm (bands W1, W2, and W3, respectively). Whenever optical counterparts were available, we used the optical coordinates for the match. WISE sources with the smallest offset from the ALFALFA coordinates were selected to be the IR counterpart. In total, 12,416 ALFALFA H I sources were detected by WISE at 3.4, 4.6, and 12 μm . Only 5,801 of these H I sources were detected by WISE at 22 μm , so only these objects are used for the [22] and [12] – [22] K-S tests. The notation [22] refers to the Vega magnitude measured at 22 μm . Results of the K-S tests are tabulated in Table 6 and indicate that H I and OH lines are significantly different in [4.6] – [12] and [3.4] – [4.6] colors.

We made cuts in WISE color and magnitude space to sep-

Table 7. Values for infrared cuts.

Infrared Cuts
[3.4] – [4.6] > 0.6
[4.6] – [12] > 3.0
[22] > 4.8
[3.4] < 15.3

Table 8. K-S tests for ALFALFA OHMs and H I line emitters after imposing the IR color and magnitude cuts listed in Table 7. The tests indicate that the OH- and H I-emitting populations can no longer be distinguished in mid-IR color/magnitude space.

Infrared Property	K-S p-value
[3.4]	0.547
[4.6]	0.136
[12]	0.016
[22]	0.748
[3.4] – [4.6]	0.258
[4.6] – [12]	0.038
[12] – [22]	0.481

arate H I from OH line emitters. Cuts were chosen to include all OHMs and exclude as many H I sources as possible; typically, the cut was made 0.1–0.2 dex above or below extremal OHM magnitudes or colors. Reducing the sample size was an iterative process: after making an initial cut and removing objects outside of the cut, we inspected the remaining sample and made a second cut in a different IR parameter. In total we made four cuts, listed in Table 7. In addition to the two colors the K-S test indicates are inconsistent, we also made cuts in [3.4] and [22]. The [3.4] and [22] magnitude cuts were able to exclude a significant number of objects from the tails of the distributions. These objects did not significantly affect the p-values of the K-S test.

High values of [3.4] – [4.6] and [4.6] – [12] color select red objects, such as IR-luminous dusty ULIRGs likely to host OHMs. The 3.4 μm band corresponds to the stellar bump from old, red stars, so the [3.4] magnitude cut selects galaxies with large stellar mass (like ULIRGs) for a fixed redshift. OHMs are luminous at 22 μm , but are distant; local H I sources could be brighter in [22] even though they are less luminous at 22 μm . So the high [22] cut removes nearby galaxies with low or moderate 22 μm luminosities. Cutting only bright 22 μm objects also avoids issues with incompleteness as it does not affect objects with low signal-to-noise in the WISE 22 μm band.

The total sample of ALFALFA H I and OH sources as well as the infrared cuts from Table 7 are plotted in Figure 4. While the [22] magnitude cut does not divide the sample to the same degree the other three cuts do, it removes ~ 50 objects that the other cuts cannot distinguish from OHMs. We also see from Figure 4 that it is not necessary to modify our simple cuts into more complex cuts involving functions of more than one IR parameter– slanted lines on the plots would not exclude a large number of additional objects. A final K-S test (Table 8) on the post-cut samples confirms that further cuts in WISE space will not significantly improve the separation of OH and H I line emitters.

ALFALFA objects that remain after the four IR cuts are plotted in color-color and color-magnitude space in Figure 5. There are 83 remaining H I sources, of which 43 are detected in WISE 22 μm . The IR cuts removed 99.3% of all H I sources and 99.3%

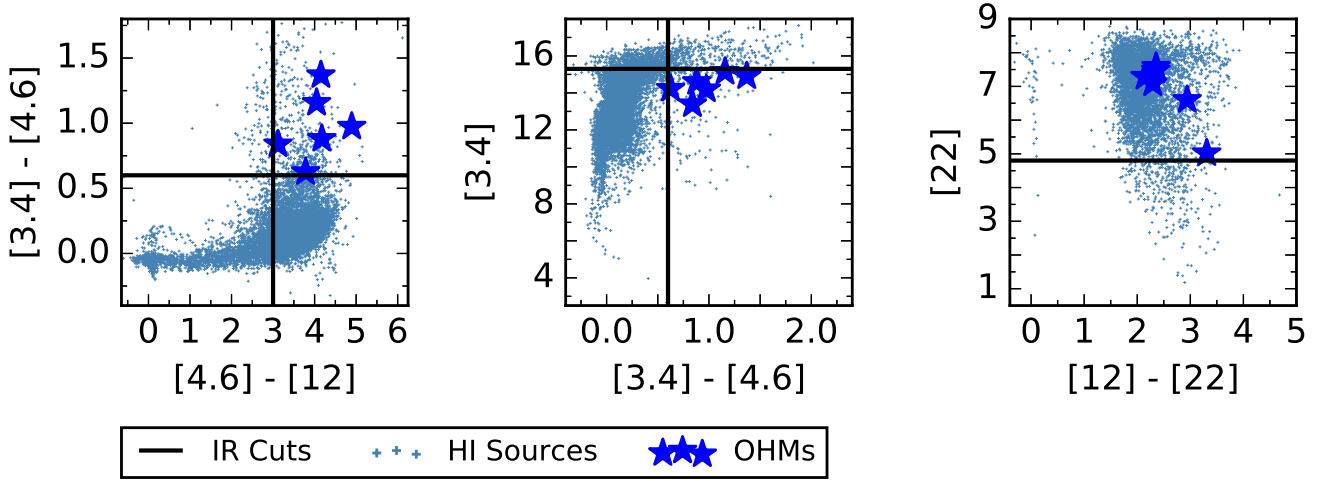


Figure 4. The total ALFALFA H I sample (blue crosses) along with ALFALFA OHMs (bright blue stars) in color-magnitude and color-color space. Black horizontal and vertical lines indicate the infrared cuts used to separate the samples (Table 7). (A color version of this figure is available in the online journal.)

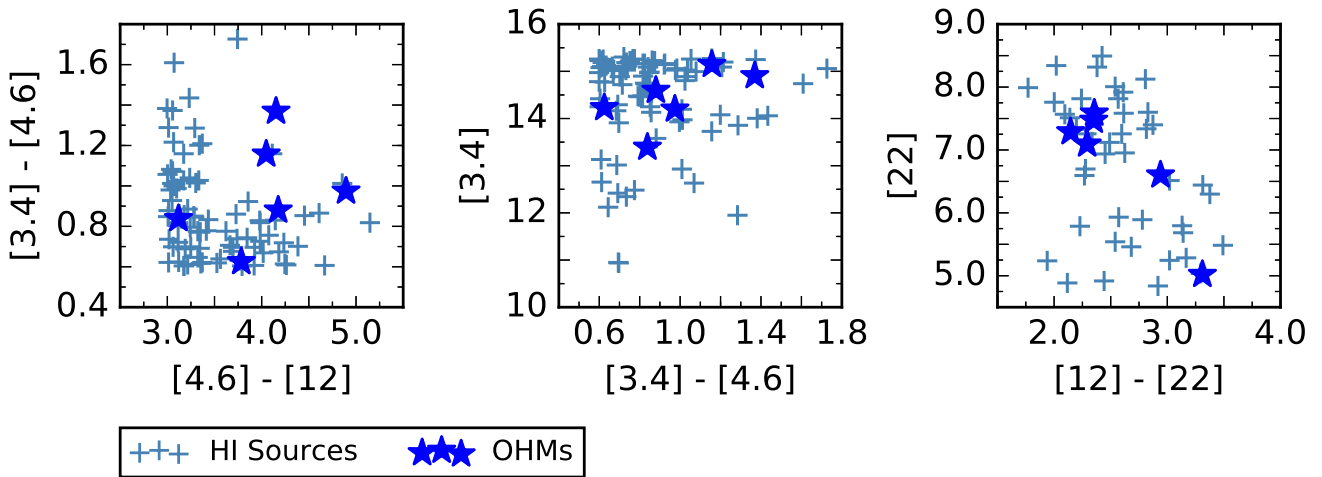


Figure 5. The post-cut ALFALFA H I sample (blue crosses) along with ALFALFA OHMs (bright blue stars) in WISE color-magnitude and color-color space. (A color version of this figure is available in the online journal.)

of H I sources detected in WISE 22 μm , increasing the fraction of OHMs in the post-cut ALFALFA sample two orders of magnitude from 4.8×10^{-4} to 6.7×10^{-2} . Other than a few H I outliers, the OH and H I detections that remain after the cuts are spread fairly uniformly across WISE space; this indicates that further cuts would not significantly improve the separation of the two populations.

4.4 ULIRG Redshift Evolution

It is necessary to introduce a redshift dependence to the magnitude and color cuts listed in Table 7 if the cuts are to be used for higher-redshift H I surveys. We used Arp 220, the closest OHM and ULIRG, as a template spectral energy distribution (SED). The SED was created using Spitzer spectra from [Armus et al. \(2004\)](#); the optical and near-IR data were fit using two stellar components (old and young), and the far-IR SED was fit using dust continuum models from [Chary & Elbaz \(2001\)](#). In Figure 6, we plot the redshift

evolution of Arp 220 and our infrared cuts in WISE color-color and color-magnitude space.

The Arp 220 tracks remain within the IR cuts for the ALFALFA OHM redshift range, $z_{\text{OH}} \leq 0.25$. The tracks above this redshift indicate how the cuts should evolve for application to planned future H I surveys. We note that the redshift evolution results in most OHMs being undetectable in the WISE 22 μm band by a redshift of $z \sim 0.4$. However, it may be possible to continue to separate H I and OH lines without use of the WISE 22 μm band or by applying the techniques used in this work to deeper IR catalogs.

5 CONCLUSIONS

In this work we identified OH megamasers in the ALFALFA H I survey, confirmed their number and IR properties matched empirical predictions based on previous surveys, and developed a method to separate OH megamasers from 99% of H I line emitters without

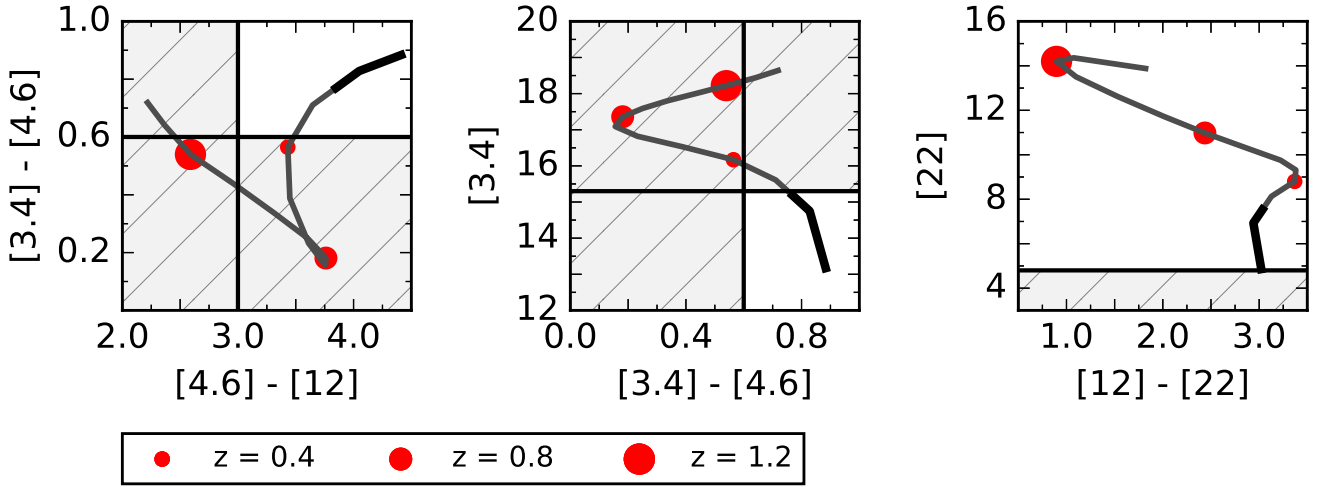


Figure 6. Track of the redshift evolution of Arp 220. Red points of increasing area mark $z = 0.4$, 0.8 , and 1.2 , while the bold portion of the track marks the ALFALFA redshift range. Horizontal and vertical black lines show the IR cuts, while the shaded region represents the quadrant or half of the plot that remains after the IR cuts. The tracks stay within the desired region through the ALFALFA redshift, $z=0.1-0.25$. Evolution past this point governs how the cuts should be adjusted for increasing redshift. (A color version of this figure is available in the online journal.)

optical spectroscopy. Optical spectroscopy of 194 candidate OHMs in ALFALFA confirmed 129 uncertain H I optical counterparts and discovered 5 new OHMs.

Only one previously known OHM lay within the survey’s volume and detection limits; this OHM was detected, raising the total number of OHMs in ALFALFA to six. Integrating the OHLF (Darling & Giovanelli 2002b) over the sky footprint, redshift range, and luminosity detection limits of ALFALFA predicts 9^{+73}_{-8} OHMs in the survey, consistent with the six detections.

Previous OHM surveys selected candidates based on IR properties; the ALFALFA OHMs are the first found in a blind spectral line survey. We used K-S tests to show that the two OHM populations come from the same statistical distribution in WISE color and magnitude as well as IRAS 60- and 100- μ m flux and FIR luminosity. This validates the IR selection criteria used in previous surveys and suggests there is no previously unknown OHM-producing environment at $z \sim 0.2$.

We used the WISE All-Sky Source Catalog to determine if OH line emitters can be distinguished from H I line emitters without the use of optical spectroscopy. This is of particular interest for planned high-redshift H I surveys, as the percentage of OH lines in an H I survey is expected to increase with redshift and reach $\sim 50\%$ by $z = 1$ (Briggs 1998). K-S tests confirm that the ALFALFA H I and OH populations can be distinguished in WISE color and magnitude space, and four IR cuts (Table 7) reduce the total number of H I objects from 12,416 to 83 and the number of H I objects detected in WISE 22 μ m from 5,801 to 43, excluding 99.3% of the ALFALFA H I sample. After the cuts, K-S tests could not distinguish the OH and H I populations; this indicates further cuts in WISE space cannot further separate the two populations. It is possible that the OHM fraction could be increased using additional data such as galaxy morphology. The redshift evolution of the closest OHM, Arp 220, provides guidelines for adjusting the WISE color and magnitude cuts for higher-redshift H I surveys. However, the sensitivity of the WISE 22 μ m band precludes the use of a [22] μ m cut at $z \gtrsim 0.4$. While a separation scheme based only on WISE data can distinguish OH from H I, future work should investigate a sep-

aration scheme using additional data sources before the advent of high-redshift H I surveys.

ACKNOWLEDGMENTS

We thank the ALFALFA observing team as well as A. Truebenbach, who provided assistance calculating ULIRG redshift evolution. We thank the anonymous referee for helpful comments that substantially improved this manuscript. This work is based on observations made at the Apache Point Observatory, operated by New Mexico State University. Support for this work was provided by a grant from the Undergraduate Research Opportunities Program at the University of Colorado, Boulder and a CASA undergraduate research grant. RG, MPH and the ALFALFA team at Cornell have been supported by NSF grants AST-0607007 and AST-1107390 and by grants from the Brinson Foundation. This research has made use of the NASA/IPAC Extragalactic Database (NED) which is operated by the Jet Propulsion Laboratory, California Institute of Technology, under contract with the National Aeronautics and Space Administration. This publication has made use of data products from the Wide-field Infrared Survey Explorer, which is a joint project of the University of California, Los Angeles, and the Jet Propulsion Laboratory/California Institute of Technology, funded by the National Aeronautics and Space Administration as well as data products from the Infrared Astronomical Satellite. This research also benefitted greatly from images provided by the Sloan Digital Sky Survey.

REFERENCES

- Armus, L., V. Charmandaris, H. W. W. Spoon, J. R. Houck, B. T. Soiffer, et al., 2004, *ApJS*, 154, 178
- Baan, W. A., P. A. D. Wood., A. D. Haschick, 1982, *ApJ*, 260, L49-L52
- Baan, W. A., A. D. Haschick, J. T. Schmelz, 1985, *ApJ*, 298, L51-L54
- Baan, W. A., J. J. Salzer, & R. D. LeWinter, 1998, *ApJ*, 509, 633-645
- Briggs, F. H., *A&A*, 336, 815-822
- Chary, R. & D. Elbaz, 2001, *ApJ*, 556, 562-581

- Clements, Sutherland et al., 1996, MNRAS, 277, 447-497, 1996.
- Darling, J. & R. Giovanelli, 2000, AJ, 119, 3003-3014
- Darling, J. & R. Giovanelli, 2001, AJ, 121, 1278-1293
- Darling, J. & R. Giovanelli, 2002a, AJ, 124, 100-126
- Darling, J. & R. Giovanelli, 2002b, AJ, 572, 810-822
- Darling, J., 2007, ApJ, 669, L9-L12
- Fullmer, L. & C. Lonsdale, 1980, (Pasadena: JPL)
- Giovanelli, R., M. Haynes, B. Kent, et al., 2005, AJ, 130, 2598-2612
- Haynes, M. P., R. Giovanelli, A. M. Martin, K. M. Hess, A. Saintonge, et al., 2011, AJ, 142, 142-170
- Hinshaw, G. F., E. Komatsu, D.N. Spergel, C. L. Bennett, J. Dunkley, et al., 2013, ApJS, 208, 20B
- Holwerda, B. W., S.-L. Blyth, A. J. Baker, 2011, The Spectral Energy Distribution of Galaxies Proceedings IAU Symposium, 284
- Johnston, S., R. Taylor, M. Bailes, N. Bartel, C. Baugh et al., Experimental Astronomy, 22, 3, 151-273
- Norris, R. P., F. F. Gardner, J. B. Whiteoak, 1998, MNRAS, 237, 673-681
- Robishaw, T., E. Quataert, & C. Heiles, 2008, ApJ, 680, 981-998
- Saintonge, A., 2007, AJ, 133, 2087-2096
- Saunders, W., W. J. Sutherland, S. J. Maddox, O. Keeble, S. J. Oliver et al., 2000, MNRAS, 317, 55-63
- Staveley-Smith, L., R. P. Norris, J. M. Chapman, D. A. Allen, J. B. Whiteoak, A. L. Roy, , 1992, MNRAS, 258, 725-737
- Wright, E. L., 2006, Publications of the Astronomical Society of the Pacific, 118, 1711-1715
- Wright, E. L., P. R. M. Eisenhardt, A. K. Mainzer, M. E. Ressler, R. M. Cutri, et al., 2010, AJ, 140, 1868-1881

This paper has been typeset from a $\text{\TeX}/\text{\LaTeX}$ file prepared by the author.